van der Pol behavior of relaxation oscillations in a periodically driven thermionic discharge

T. Klinger, F. Greiner, A. Rohde, and A. Piel
Institut für Experimentalphysik, Christian-Albrechts-Universität Kiel, Olshausenstraße 40-60, D-24098 Kiel, Germany

M. E. Koepke
Department of Physics, West Virginia University, Morgantown, West Virginia 26506-6315
(Received 24 May 1995)

The nonlinear dynamics of the frequency entrainment process in periodically driven, self-oscillating thermionic discharges is investigated experimentally. The periodically interrupted frequency entrainment process, known as periodic pulling, is demonstrated to be an essential feature of the transition region between the quasiperiodic state and the entrained state. A detailed comparison of experimental findings with the analytical and numerical study of the driven van der Pol equation $\ddot{x} - \epsilon(1 - \beta x^2)\omega_0 \dot{x} + \omega_0^2 x = \omega_0^2 E \cos(\omega_i t)$ confirms the relevance of this dynamical model for nonlinear plasma oscillations. A physical explanation is developed based on results from particle-in-cell simulations of periodic pulling in thermionic discharges.

PACS number(s): 52.35.−g, 52.75.Fk, 05.45.+b

I. INTRODUCTION

Simple mathematical models are often helpful for the understanding of nonlinear dynamical phenomena of physical systems. In particular, the detailed dynamical behavior of oscillatory unstable systems is generally well described by an appropriately chosen nonlinear oscillator model (see Ref. [1] for an overview on recent experimental and theoretical work). A classical nonlinear oscillator model is the van der Pol (vdP) model [2]. It is described by a second-order differential equation with a nonlinear friction term. As one of its most prominent features, stable limit cycles in phase space are established, emerging from a subtle balance between energy gain and dissipation. This belongs to a time evolution characterized by a self-excited relaxation oscillation process governed by two distinct time scales: a slow filling phase and, after a certain threshold condition is met, a rapid reorganization of the initial state. van der Pol already has considered the periodically forced variant of his model [3], whose dynamical behavior is mainly characterized by quasiperiodicity and frequency entrainment [4]. Frequency entrainment allows the oscillation frequency to shift to that of an external periodic driving force and many technical applications have been found (cf., for example, [5]). Recently, the nonlinear dynamics of the periodically driven vdP oscillator has attracted new attention. The occurrence of a blue sky catastrophe [6], the devil's staircase [7], and period-doubling bifurcations towards chaos in synchronized states [7,8] are only a few examples of its newly discovered more complex dynamical features.

The interpretation of resonance effects in externally modulated gas discharge systems has often benefited by comparison with the driven vdP model. For periodically driven collisional ion sound waves, the vdP equation has been derived starting from the basic set of ion fluid equations [9,10]. Other examples for the successful application of the driven vdP model to resonance phenomena in plasma physics are beam-plasma systems [11–13], ionization waves [14,15], and potential relaxation oscillations [16,17]. However, even the vdP model has its limitations and in some cases, considerable modifications are necessary for a convincing agreement between experimental observation and the oscillator model [18,19].

A rarely noticed but nevertheless important dynamical feature of the driven vdP model is the so-called periodic-pulling phenomenon [20]. Briefly described, it is a periodically repeated incomplete frequency entrainment process. This leads to significant modifications of the resulting time series, power spectra, and phase-space structure [21]. As discussed in Ref. [22], this can give rise to misleading or incorrect interpretations as sideband suppression or intermittency. The periodic-pulling phenomenon has been demonstrated to be of great importance for the dynamical behavior of unijunction transistor oscillators [21], microwave oscillators [5], neon bulb relaxation oscillators [23], but also different kinds of plasma waves in laboratory [22,24–26] and fluctuations in the earth's magnetosphere [27].

In this paper we present a detailed numerical and experimental investigation of the periodic-pulling phenomenon in a periodically driven self-oscillating thermionic discharge. In a certain operation regime, the thermionic low-pressure discharge with volume ionization performs strong, relaxationlike current oscillations that can be classified as a close relative of the potential relaxation instability [28,29]. Recently, the nonlinear dynamics of such self-excited plasma oscillations have been studied in detail by a comparison between computer simulation and experiment [30–32]. In these papers a model description for the self-oscillations has been established. This model reveals the physical mechanisms of the nonlinear dynamical behavior of the periodically forced

thermionic discharge. Period-doubling bifurcations and frequency entrainment of the oscillating discharge have been studied and have been compared with the theory of sine circle map dynamics. However, the nonlinear dynamical phenomena related to frequency entrainment are much more subtle than described by the circle map. The rich behavior observed in the experiment needs the more careful analysis presented in this paper: The analytical treatment of periodic pulling (Sec. II) is completed by a numerical solution of the vdP equation (Sec. III). The self-oscillating thermionic discharge is investigated experimentally (Sec. IV) and the physical mechanism of the observed dynamical phenoma is discussed on the basis of particle-in-cell simulations (Sec. V). The present study provides a detailed understanding of the dynamical behavior of a periodically driven discharge plasma.

II. ANALYTICAL TREATMENT OF PERIODIC PULLING

As already outlined above, the van der Pol oscillator is a model for nonlinear relaxation oscillators. The periodically driven vdP oscillator is given by the equation

$$\frac{d^2x}{dt^2} - \epsilon\left(1-\beta x^2\right)\omega_0\frac{dx}{dt} + \omega_0^2 x = \omega_0^2 E\cos(\omega_i t)\,, \qquad (1)$$

where ϵ is a parameter that determines the degree of nonlinearity, β characterizes the degree of nonlinear saturation, and $f_0 = \omega_0/2\pi$ is the frequency of the free-running oscillator. The (injected) driving force has frequency $f_i = \omega_i/2\pi$ with amplitude E. The trial solution of Eq. (1),

$$x(t) = a(t)\sin[\omega_i t - \phi(t)], \qquad (2)$$

includes the time evolution of both amplitude $a(t)$ and relative phase $\phi(t)$ between the driving force and the system response. Lashinsky [20] has derived differential equations for slowly varying $a(t)$ and $\phi(t)$ and weak nonlinearity ϵ using the method of harmonic balance [33]. A simplification is possible if the driving frequency is restricted to small deviations from the free-running frequency, $(\omega_0^2 - \omega_i^2)/2\omega_i \approx \omega_i - \omega_0$. The result is found to be

$$\frac{da}{dt} = \frac{\epsilon\omega_0 a}{2}\left[1-\left(\frac{a}{a_0}\right)^2\right] + \frac{E}{2}\frac{\omega_0^2}{\omega_i}\cos\phi, \qquad (3a)$$

$$\frac{d\phi}{dt} = \Omega_0 - \frac{E}{2a}\frac{\omega_0^2}{\omega_i}\sin\phi\,. \qquad (3b)$$

Here, $a_0 = 2/\sqrt{\beta}$ denotes the equilibrium amplitude of the free-running vdP oscillator, and $\Omega_0 = \omega_i - \omega_0$ is the conventional beat frequency. By introducing the dimensionless entrainment parameter

$$\alpha = \frac{E}{2a}\frac{1}{(\omega_0/\omega_i) - 1}\,, \qquad (4)$$

Eq. (3b) can be rewritten in the form

$$\frac{d\phi}{dt} = \Omega_0[1 - \alpha\sin\phi]\,. \qquad (5)$$

In an entrained state, the relative phase ϕ is independent of time. This implies the condition $|\alpha| \geq 1$. The vdP oscillator is entrained by the external force if α reaches unity if

$$\frac{\omega_i}{\omega_0} - 1 = \frac{E}{2a}\,. \qquad (6)$$

For nonzero driving force E entrainment occurs for $\omega_i \neq \omega_0$. The entrainment condition (6) is met either by increasing the driving force E or by decreasing the frequency difference Ω_0. Equation (5) has been derived independently by Adler [34] using arguments from system theory. It can be integrated analytically and the solution is

$$\tan\frac{\phi(t)}{2} = \sqrt{1-\alpha^2}\,\tan(\Omega_0\sqrt{1-\alpha^2}\,t/2) + \alpha\,. \qquad (7)$$

The beat frequency Ω of $\phi(t)$ is obtained from the periodicity of $\tan(\phi/2)$,

$$\Omega = \Omega_0\sqrt{1-\alpha^2} = \Omega_0\sqrt{1-(E/E_c)^2}\,, \qquad (8)$$

where $E_c \equiv 2a\Omega_0/\omega_0$ is the forcing amplitude associated with the onset of entrainment, a relationship recently verified by experiment [21]. The complex phase factor $\exp(i\phi)$ with ϕ given by Eq. (7) can be expressed in the form [35]

$$\exp[i\phi(t)] = \frac{1}{i\tan\frac{\Theta}{2}} \times\left[\frac{1-\tan^2\frac{\Theta}{2}}{1-i\tan\left(\frac{\Theta}{2}\right)\exp\,i(\Omega t+\Theta)}\right], \qquad (9)$$

where Θ is fixed by the relations $\Omega = \Omega_0\cos\Theta$ and $\sin\Theta = \alpha$. Expression (9) is the phase factor of the complex continuation of Eq. (2),

$$x(t) = a\exp i[\omega_i t + \phi(t)], \qquad (10)$$

and can be developed into a Fourier series

$$\exp i\phi(t) = \sum_{-\infty}^{+\infty} c_n \exp\,i(n+1)\Omega t \qquad (11)$$

for $\omega_i > \omega_0$ ($\omega_i < \omega_0$) with the coefficients

$$c_n = \begin{cases} 0 & \text{for} \quad n < -1 \quad (n \geq 0) \\ i\tan\frac{\Theta}{2} & \text{for} \quad n = -1 \quad (n = -1) \\ \left(1-\tan^2\frac{\Theta}{2}\right)\left(i\tan\frac{\Theta}{2}\right)^n e^{i(n+1)\Theta} & \text{for} \quad n \geq 0 \quad (n < -1)\,. \end{cases} \qquad (12)$$

Here c_n is the nth component of a sideband structure $\omega_{sn} = \omega_i + (n+1)\Omega = 2\pi f_{sn}$ that is referenced to the driving frequency ω_i. The resulting power spectra and the time evolution of the relative phase are shown in Fig. 1(a) for different values of α. According to Eq. (12), the spectra are single sided with respect to ω_i. (In contrast, the sidebands ω_{sn} in the spectrum of an ordinary quasiperiodic state are symmetric.) As $|\alpha| \to 1$, the beat frequency Ω decreases and additional spectral lines appear. The amplitudes of c_n show a geometrical progression for $n > 0$, which corresponds to a linear decrease on the logarithmic scale. The time evolution of the relative phase $\phi(t)$ is shown in Fig. 1(b). For $\alpha = 0$ the phase development would be linear, as expected for conventional amplitude modulation. The increase of $|\alpha|$ increases the nonlinearity in the evolution of the phase relation which corresponds to an increasing nonsinusoidal modulation in frequency, a property recently demonstrated by experiment [36]. Close to $|\alpha| = 1$, the phase evolution can be subdivided into a slow and a fast part. The synchronous modulation of the amplitude and the frequency in the system response of a periodically forced nonlinear oscillator is a primary characteristic of this asymmetric spectral broadening process, known as periodic pulling, as emphasized by Koepke and Hartley [21].

III. NUMERICAL TREATMENT OF vdP EQUATION

The numerical solution of the periodically driven vdP equation (1) provides an independent characterization of the periodic-pulling phenomenon. For this purpose, the set of first-order differential equations for $x_1 = x$ and $x_2 = dx/dt$ in dimensionless notation,

$$\frac{dx_1}{dt} = x_2\,, \tag{13a}$$

$$\frac{dx_2}{dt} = E\cos(\nu\tau) + \epsilon(1-\beta x_1^2)x_2 - x_1\,, \tag{13b}$$

is solved numerically, where the variable $\nu = \omega_i/\omega_0$ denotes the normalized frequency and $\tau \equiv \omega_0 t$ is the dimensionless time scale. The two-dimensional projection of the phase-space trajectory is directly ob-

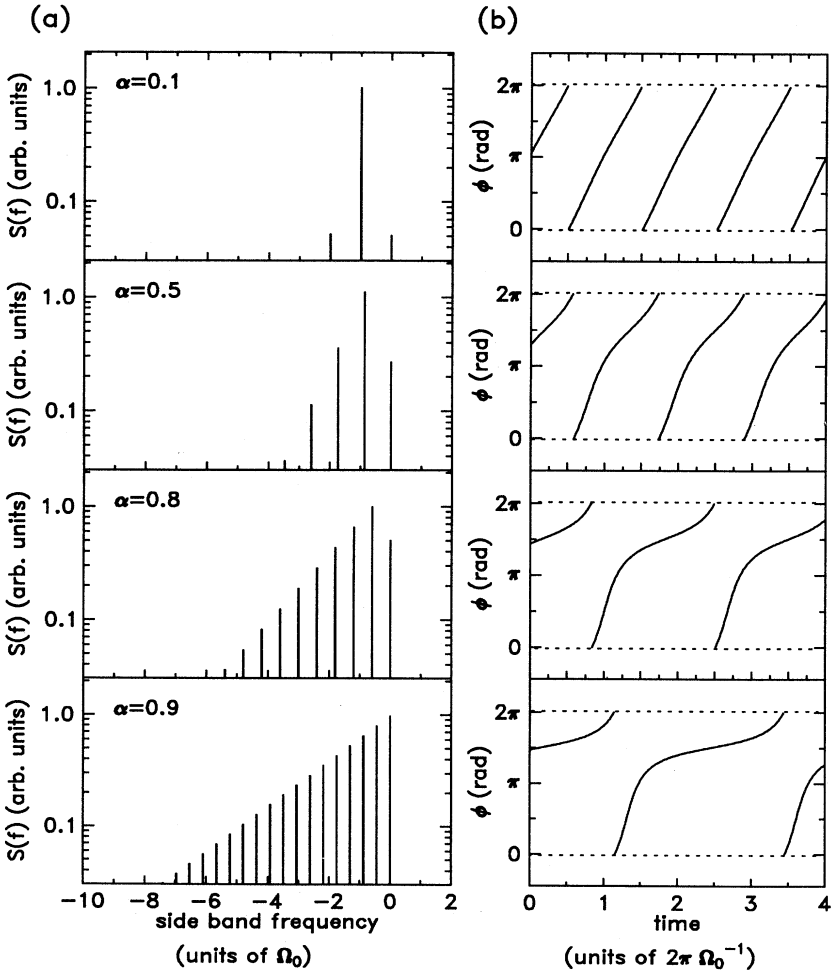

FIG. 1. Analytic theory of periodic pulling. Shown are the power spectra of the response signal on a logarithmic scale (a) and the time evolution of the relative phase between driver and response signal (b) for different values of the entrainment parameter α. From top to bottom, the periodic-pulling phenomenon gets more evident, i.e., more and more sidebands of the single-sided spectra appear and the temporal phase evolution becomes nonlinear.

tained by plotting x_1 versus x_2. The stroboscopic mapping $(x_1(nT), x_1((n+1)T))$ is sampled at times $0, T, 2T, \ldots, nT$, where $T = 2\pi/\omega_i$ is the period of the driving force. For the dynamical system under investigation, the stroboscopic mapping is topologically equivalent to the Poincaré map [37].

The bifurcation structure of the periodically forced vdP oscillator has been studied by numerical methods [7,8]. Different bifurcation classes have been found and two of the most important are saddle-node bifurcations between quasiperiodic and entrained states in the weakly driven case and period-doubling bifurcations in entrained states for the strongly driven case [8]. Areas in the $\{\nu, E\}$ plane for which the system is entrained (i.e., mode locked) are known as Arnol'd tongues [37]. The winding number w allows one to distinguish between entrained and quasiperiodic states. If the vdP oscillator is entrained by the driving force, the winding number remains constant $w = p/q$ (p, q are positive integers) over some range of ω_i. In principle, between each two locking ranges with winding numbers $w = p/q$ and $w' = p'/q'$, there exists another entrained state with winding number $w'' = (p + p')/(q + q')$. This hierarchy is known as Farey's sequence [37]. For the strongly driven, entrained oscillator, period-doubling bifurcations have been found [7,8].

In the immediate vicinity of Arnol'd tongues, periodic-pulling effects are most evident. This is illustrated by a diagram in the $\{\nu, E\}$ parameter plane for the vicinity of an Arnol'd tongue of periodicity one (Fig. 2). Lines of equal periodic pulling are given by Eq. (4) and are shown for different values of the entrainment parameter α. Without loss of generality $2a$ is set to unity. For $|\alpha| \to 1$, the oscillator performs a saddle-node bifurcation to an entrained state of periodicity one (shaded region in Fig. 2). The transition from weak to strong periodic pulling in the quasiperiodic regime, however, is smooth and should not be considered as a separate type of bifurcation. For this reason, periodic pulling is not usually recognized by commonly used bifurcation analysis tools [38], although it is an essential feature of the vdP dynamics.

In Figs. 3–5, the numerical solution of Eqs. (13a) and (13b) is shown for three different values of ν while E is kept constant. As indicated by the arrow in Fig. 2, the driving frequency ν is varied to study both weak and strong periodic pulling and the entrained state. Figures 3–5 include the two-dimensional representation of the phase space, the stroboscopic mapping, the time series of the driving force $E\cos(\omega_i t)$ and system response $x(t)$, the power spectrum $S(f)$ of the system response, and the time evolution of the phase relationship $\phi(t)$. In Fig. 3 the phase-space diagram of the quasiperiodic

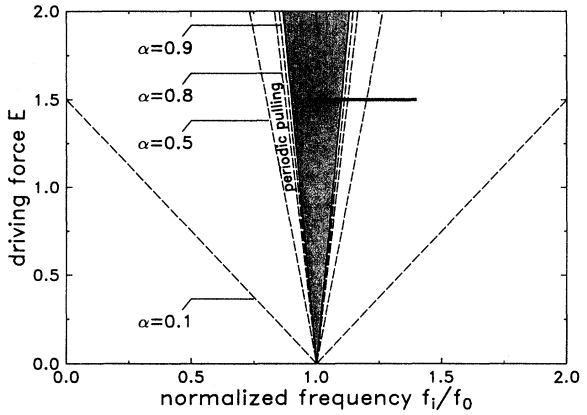

FIG. 2. Arnol'd tongue for the frequency-entrained states of periodicity one (shaded region). The dashed lines correspond to different entrainment parameters α and indicate lines of equally marked periodic pulling. The numerical and experimental investigations of the periodic-pulling phenomenon are performed by decreasing the driving frequency while the driving force is kept constant, as indicated by the arrow.

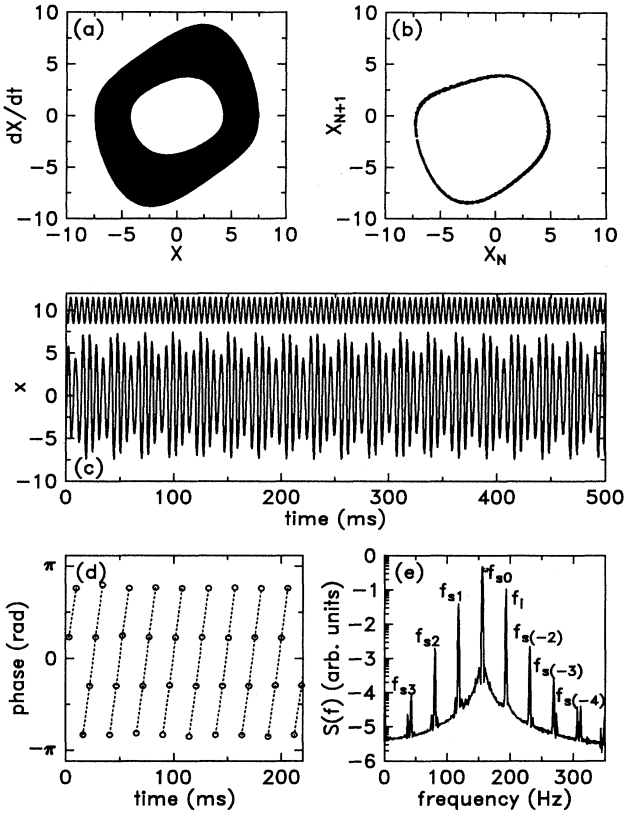

FIG. 3. Numerical solution of the forced vdP equation (13) for the case of weak periodic pulling ($\epsilon = 0.4$, $\beta = 0.1$, $E = 1.5$, $\nu = 1.2157$): Shown are (a) the two-dimensional projection of the phase space $\{x, \dot{x}\}$, (b) the stroboscopic mapping, (c) the time series of the system response (trace below) and driving force (trace above, vertically shifted for clarity), (d) the time evolution of the relative phase between driver signal and system response, and (e) the response power spectrum.

state shows the projection of a two-torus. Consequently, the stroboscopic mapping is a closed cycle. The system response shows a moderate amplitude modulation of $\approx 63\%$ for the ratio of minumum to maximum of the wave envelope. In the power spectrum, a spectral feature at f_{s0} associated with and appoximately equal to the free-running frequency f_0 is found. The driving frequency f_i is seen, as well as sidebands f_{sn} due to the nonlinear interaction.

If the driving frequency is chosen close to an Arnol'd tongue, pronounced periodic pulling is found in the dynamical behavior of the system, as indicated in Fig. 4. The phase-space trajectory no longer homogeneously covers the surface of the two-torus but instead fills its center. Accordingly, the stroboscopic mapping has regions with significantly different point densities. The system's response now shows both amplitude and frequency modulation. The amplitude modulation is strongly nonsinusoidal and the modulation depth has strongly increased, while the driving force amplitude E has remained fixed. This exaggerated amplitude modulation is a consequence of the rapid readjustment of phase during the interruption of the frequency pulling process between each beat cycle. Such a phase readjustment can be recognized in the system response in Fig. 4(c) at $t = 35, 185$, and 335 ms, where the readjustment eliminates approximately 180° of relative phase with respect to the driving force as indicated in the phase evolution in Fig. 4(d). The power spectrum is asymmetric with respect to f_i, consistent with the analytical results outlined earlier. In Fig. 5, entrainment is achieved by decreasing the driving frequency. The phase-space trajectory is a limit cycle, the stroboscopic mapping is a fixed point, modulation is absent in the system response, and the power spectrum indicates only monochromatic harmonics of $f_{s0} = f_i$.

Apart from the well-understood bifurcation structure, the periodic-pulling phenomenon plays an important role in the transition regime between quasiperiodic and entrained states of the vdP oscillator. The analytical and numerical results are completely consistent. Thus the vdP oscillator can be considered as a paradigm for driven relaxation oscillations in experimental situations. Such a

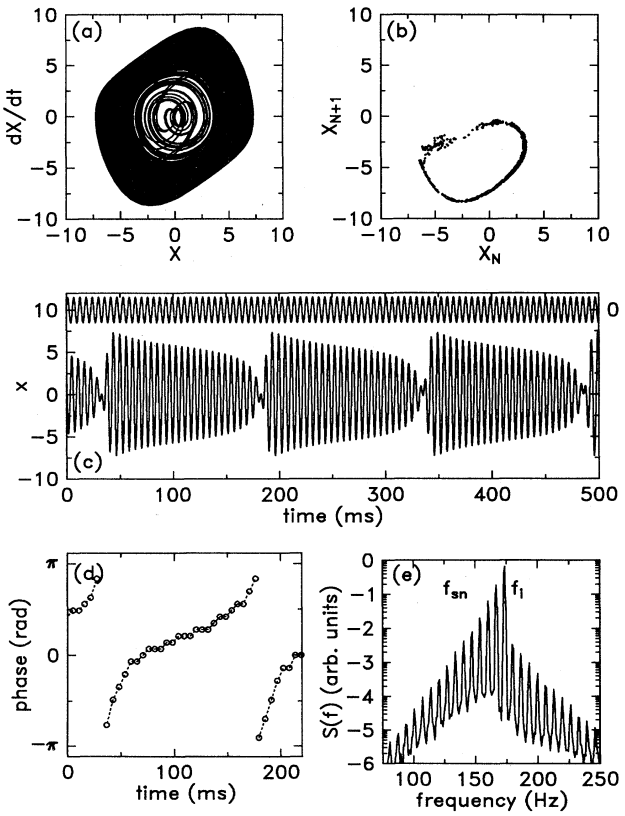

FIG. 4. Numerical solution of the forced vdP equation (13) for the case of strong periodic pulling. ($\epsilon = 0.4$, $\beta = 0.1$, $E = 1.5$, $\nu = 1.09$): (a) the phase space $\{x, \dot{x}\}$, (b) the stroboscopic mapping, (c) the time series of the system response (below) and driving force (above, vertically shifted for clarity), (d) the phase evolution, and (e) the response power spectrum.

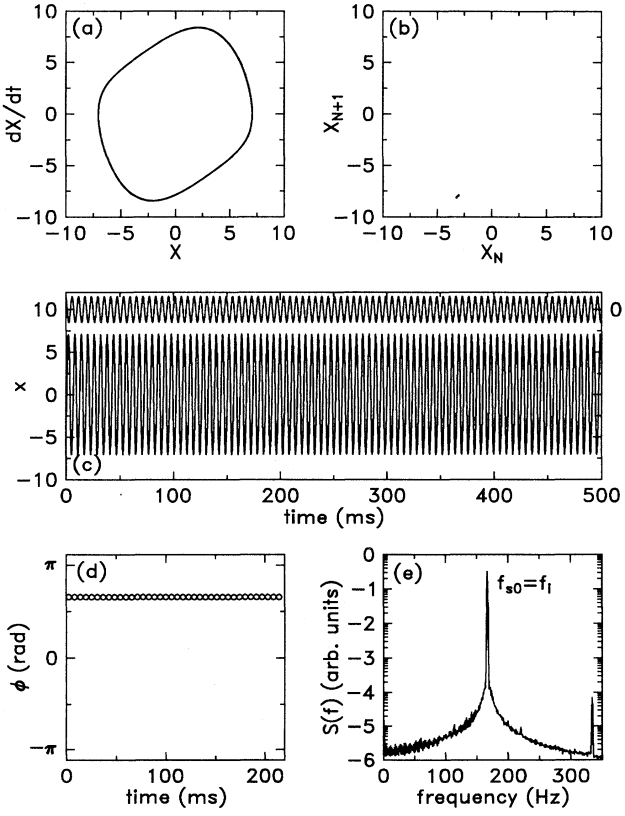

FIG. 5. Numerical solution of the forced vdP equation (13) for the case of entrainment. ($\epsilon = 0.4$, $\beta = 0.1$, $E = 1.5$, $\nu = 1.05$): (a) the phase space $\{x, \dot{x}\}$, (b) the stroboscopic mapping, (c) the time series of the system response (below) and driving force (above, vertically shifted for clarity), (d) the phase evolution, and (e) the response power spectrum.

paradigm allows one to classify the dynamical features of periodic pulling.

IV. EXPERIMENT

Experimental investigations have been carried out in a magnetized thermionic discharge with filament cathode. An axial, homogenous magnetic field B (≤ 27 mT) confines the electrons and, to a good approximation, constrains their motion to one dimension between anode and cathode. This allows a direct comparison of experimental results with the interpretation of one-dimensional computer simulations [31,32]. The experimental arrangement is shown in Fig. 6. A cylindrical stainless-steel vacuum vessel, 15 cm in diameter and 1 m in length, lies inside a set of ten magnetic field coils. The filling gas is argon at a pressure $p \approx 0.1$ Pa. The mean free paths for electron-neutral collisions (ionization) and ion-neutral collisions (charge exchange) are comparable to the discharge length.

Two different stable discharge modes can be established [30]: the low-current anode-glow mode (AGM) and the high-current temperature-limited mode (TLM). They can be distinguished by the axial potential structure (Fig. 7) that is directly measured with movable emissive probes [39]. In the transition region between the AGM and the TLM, nonlinear relaxation-type oscillations in both discharge current $I_d(t)$ and plasma potential occur. The experimentally determined $\bar{I}_d(U_d)$ characteristic (the overbar indicates a time-averaged discharge current, U_d is the discharge voltage) and the time series of the discharge current is shown in Figs. 7(a) and 7(c). For values of U_d above the ionization potential and below 17.5 V, the AGM is established. Relaxation oscillations are observed for 17.5 V $\leq U_d \leq$ 28 V and, for $U_d >$ 28 V, the discharge performs an abrupt transition to the TLM. Note the pronounced hysteresis in the $I_d(U_d)$ characteristic between the AGM and the TLM [40].

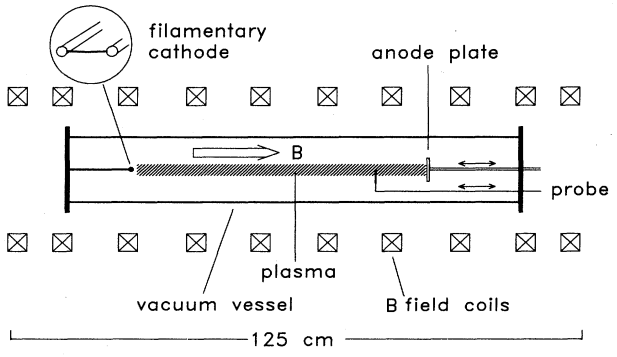

FIG. 6. Schematic diagram of the magnetized thermionic low-pressure discharge. A directly heated tungsten filament is the cathode. The discharge length is given by the axial anode position. The axial potential distribution is measured by movable emissive probes. The plasma is confined by a homogeneous axial magnetic field.

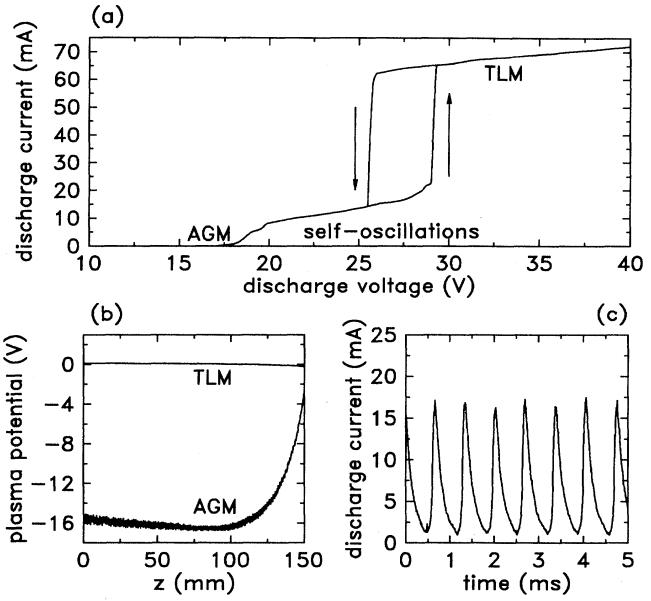

FIG. 7. Properties of the thermionic discharge at low pressure: (a) hysteresis in the discharge voltage–discharge current characteristic, (b) axial potential structure in the strong current temperature-limited mode (TLM) and anode-glow mode (AGM), (c) time series of strong relaxation oscillations in the discharge current occurring in the transition regime between AGM and TLM.

For thermionic discharges at low pressure, the mechanisms of stable discharge modes and self-oscillations have recently been studied in detail using particle-in-cell simulations [31,32,30]. The results can be summarized as follows: The AGM is essentially a discharge state with a space-charge limited electron current from the cathode. Under certain conditions, the cathodic plasma region is the subject of a Pierce instability [41]. As a consequence, strong potential structures are generated that accelerate ions into the region of negative space charge. This leads to a sudden increase in the discharge current, followed by a gradual decay of the discharge current. The time scale of the decay is set by the ion transit through the discharge. This process repeats periodically. The oscillation phenomenon can be considered as a category of potential relaxation oscillations [28,29].

The self-oscillating discharge is modulated externally to investigate its nonlinear dynamical behavior. An electronically controllable power supply allows the modulation of the discharge voltage at constant circuit impedance. The time variation of the discharge current $I_d(t)$ is a good representation of the system's response to the external periodic perturbation. A variety of entrained states with different winding numbers w can be found as the value f_i/f_0 is varied. In Fig. 8, experimentally determined Arnol'd tongues are presented for subharmonic ($w > 1$) and higher harmonic entrainment ($w < 1$). The driving modulation degree m_d, defined

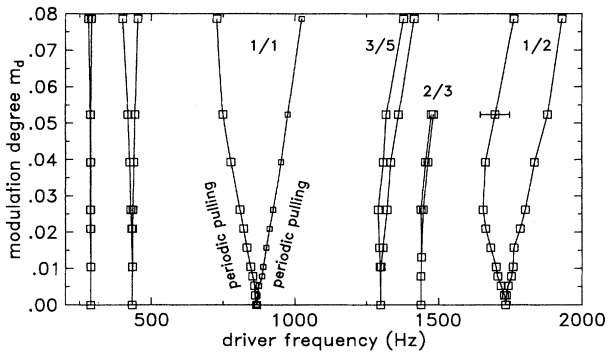

FIG. 8. Arnol'd tongues in the subharmonic and superharmonic regimes for the weakly driven discharge (modulation degree $m_d = \delta U_d/U_d \leq 0.08$). The frequency of the unperturbed self-oscillations is $f_0 = 870$ Hz. The winding number $w = P/Q$ in frequency-entrained states is indicated for the Arnol'd tongues in the superharmonic regime by integer numbers for P and Q. In the close vicinity of Arnol'd tongues strong periodic pulling occurs.

as the ratio of the modulation signal (peak to peak) to the average discharge voltage $U_d(t)$ is less than 8%. For this weak modulation, the system performs saddle-node bifurcations between quasiperiodic and entrained states. Because of the relatively low coherency of the self-oscillations, the complete set of possible Arnol'd tongues cannot be resolved. Nevertheless, the observed Arnol'd tongues follow the Farey sequence. For strong modulation degree $m_d > 25\%$, it has been demonstrated that period-doubling bifurcations towards chaotic behavior occur [42,30,32].

For the following discussion of periodic pulling, we restrict ourselves to the neighborhood of the Arnol'd tongue associated with the harmonic ($w = 1/1$) entrainment (Fig. 8) of the self-oscillation process by the external modulation of the discharge voltage. To study the detailed dynamics of the entrainment process, we start from a quasiperiodic state and approach the Arnol'd tongue by decreasing the driving frequency while the modulation degree is kept constant. The result is shown in Figs. 9–11. The power spectrum in a quasiperiodic state [Fig. 9(a)] has three qualitatively different components: the driving frequency f_i, the frequency f_{s0} associated with the free-running frequency, and sidebands $f_{sn} = f_{s0} + n\Omega$. The system response [Fig. 9(b)] shows a weak modulation and the evolution of the phase difference between the driving force and the response [Fig. 9(c)] is approximately linear. Both the modulation and the phase evolution have a periodicity given by the beat frequency $\Omega = 170$ Hz. Periodic pulling becomes more evident as the Arnol'd tongue is approached: The triangular power spectrum in Fig. 10(a) is more asymmetric with respect to f_i. The synchronized amplitude and phase modulation, responsible for the sideband cancellation effect described in Sec. II, is revealed in the time series of the system response and the phase evolution $\phi(t)$ [Figs. 10(b) and 10(c)]. As predicted by the theory of periodic pulling, an alternating sequence of fast (first 1/4 of each beat cycle) and slow (last 3/4 of each beat cycle) changes in the phase is observed. In addition, the amplitude modulation in the system response is nonsinusoidal. In the entrained state, shown in Fig. 11, the power spectrum consists only of a single pronounced component at f_i. The system response is now phase locked to the driving force, i.e., the phase relation between driving force and the response is constant in time.

The prediction discussed in Sec. II, that the spectral asymmetry changes as $\alpha \to 1$, is demonstrated experimentally in Fig. 12(a) by a stepwise increase of the modulation degree m_d, while the driving frequency is held constant. The sequence of power spectra begins with a quasiperiodicity case associated with negligible periodic pulling. For increased modulation degree, the beat frequency Ω decreases and the spectra become more asymmetric with an increasing number of sidebands at $f_{sn} < f_i$. Above the critical α value $\Omega = 0$ (not shown). The qualitative shape of the experimentally determined spectra agrees with that in Fig. 1. The periodic-pulling phenomenon significantly influences the appearance of the stroboscopic mapping of the system response [Fig. 12(b)].

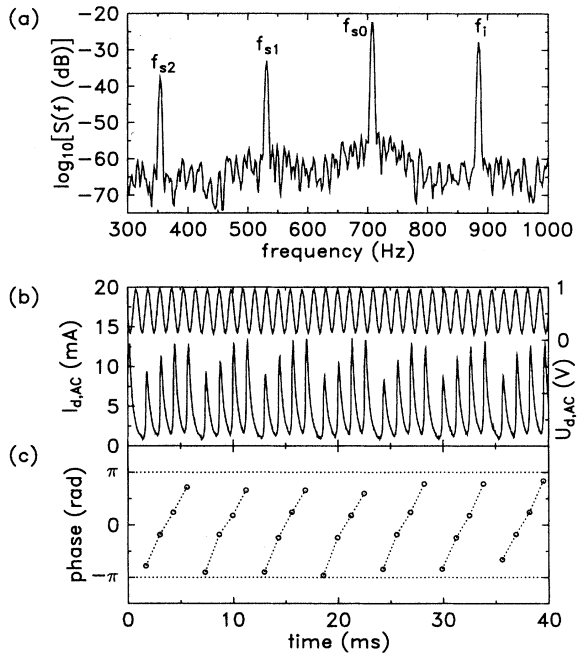

FIG. 9. Experimentally determined quasiperiodic state at large distance from any Arnol'd tongue. The driving frequency in the present case is $f_i = 885$ Hz, the zeroth-order sideband is located at $f_{s0} = 707$ Hz. Shown are (a) the time-averaged power spectrum of the discharge current fluctuations, (b) time series of the driver signal superimposed on the discharge voltage (top trace) and the discharge current as the system's response (bottom trace), and (c) the time evolution of the relative phase between driver signal and reponse signal. No evidence for periodic pulling is found in the power spectrum, the time series, and in the phase evolution.

The homogeneity with which the phase-space two-torus is covered is reduced as $|\alpha| \to 1$ until a fixed point in the stroboscopic mapping is approached. The assembly of points in the lower right corner of the diagrams in Fig. 12(b) corresponds to the very small amplitude of the nodes of the distorted beats. The beat frequency Ω, as given by Eq. (8), is determined from the observed power spectra. It is compared with the conventional beat frequency Ω_0 for a horizontal cut (i.e., for constant modulation degree) across an Arnol'd tongue and its neighborhood, as shown in Fig. 13(a), and for a vertical cut (i.e., for constant driving frequency) across the Arnol'd tongue boundary and its neighborhood in Fig. 13(b). Within experimental uncertainty due to stochastic fluctuations of the driven system, the experiment agrees much better with vdP theory of periodic pulling than with a linear model, especially in the vicinity of the Arnol'd tongue.

V. SIMULATIONS

Particle-in-cell (PIC) simulations can be of great value for the physical interpretation of the nonlinear dynamical behavior of thermionic discharges [43]. As mentioned above, the descriptive model [31] of relaxation oscillations of the low-pressure thermionic discharge with filament cathode has been developed from PIC simulations. This model is also suitable to provide a physical understanding of entrainment by periodic external modulation.

In this section simulation results of periodic-pulling phenomena are discussed. Simulations are carried out with the PDP1 code of Birdsall and co-workers [44,45]. Simulation parameters are chosen to match the experimental conditions as closely as possible, except for a low ion-to-electron mass ratio, $\mu = m_i/m_e = 10$, which is used to save computing time. It had been demonstrated before that dynamical features of the simulated discharge remain unaffected by the choice of the mass ratio [46,31].

In the simulation, the plasma potential is slightly preferred over the discharge current as a representation of the system's response. One reason for this preference is the information it provides on the time history of local potential structures. As in the experiment, the discharge voltage of the self-oscillating system is modulated externally at a frequency f_i with a moderate modulation degree. The time series and the corresponding power spectrum are shown in Fig. 14. The modulation of the plasma

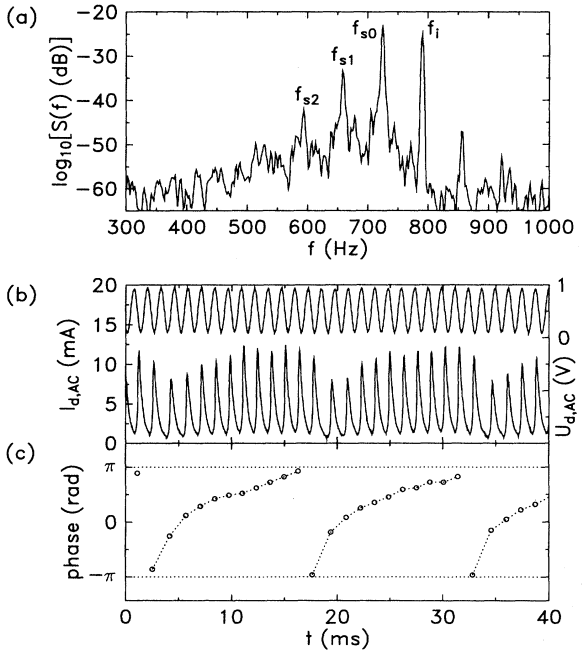

FIG. 10. Experimental observation of strong periodic pulling. The driving frequency is $f_i = 790$ Hz, the zeroth-order sideband is located at $f_{s0} = 727$ Hz. Shown are (a) the time-averaged power spectrum of the discharge current fluctuations, (b) time series of the driver signal superimposed on the discharge voltage (top trace) and the discharge current as the system's response (bottom trace), and (c) the time evolution of the relative phase between driver signal and reponse signal. The characteristic features of periodic pulling are obvious: The power spectrum is almost single sided, the envelope of the system's response is strongly nonsinusoidal, and the phase evolution is far from being linear.

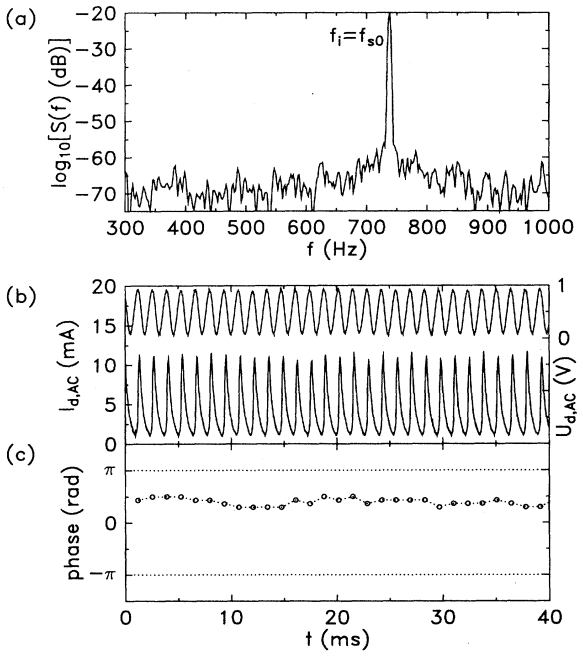

FIG. 11. Frequency-entrained state of periodicity one in the experimental discharge system. The driver frequency and the zeroth-order sideband are identical, $f_d = f_{s0} = 738$ Hz. Shown are (a) the time-averaged power spectrum of the discharge current fluctuations, (b) time series of the driver signal superimposed on the discharge voltage (top trace) and the discharge current as the system's response (bottom trace), and (c) the time evolution of the relative phase between driver signal and reponse signal. The small fluctuations in the phase evolution are due to noise.

potential is nonsinusoidal and has an asymmetric spectrum. As expected from theory, the number and height of sidebands are larger on one side of f_i than on the other side, causing the spectrum to become more asymmetric. The detailed structure of the power spectra is slightly obscured by the inherent low coherency of the simulated self-oscillation process. Nevertheless, the average beat period is given by $2\pi/\Omega$. The properties of the time series and the power spectrum are unambiguous signatures of periodic pulling in the simulated discharge system.

A more detailed view of two beat cycles for the same simulation parameters as of Fig. 14(b) is shown in Fig. 15. To make clear the phase evolution of the system response, the appropriately scaled driving-force is included in the diagram as a dashed line. Each beat cycle has the length of five driving force periods. The sharp peaks in the time series of the potential indicate the sudden rise of a transient double layer in the discharge, that causes a steep increase of the discharge current (see Sec. IV). In Fig. 15, the arrows define the beginning and end of a particular beat cycle. At the beginning of a cycle, peaks in the plasma potential occur with a frequency that is pulled toward the driving frequency without reaching it. The residual frequency difference results in a phase difference that slowly accumulates throughout the beat cycle. When the phase difference is sufficiently large, the frequency pulling is interrupted and the phase difference rapidly readjusts to repeat the process. In Fig. 15, this readjustment occurs between the fourth and the fifth driving-force periods. This process corresponds to a nonsinusoidal frequency modulation of the system response.

The most pronounced event during each beat cycle is indicated in Fig. 15 also by the arrows. During period 5, the instability in the potential structure occurs at the maximum in discharge voltage magnitude. This particular phase relation is always observed in entrained states

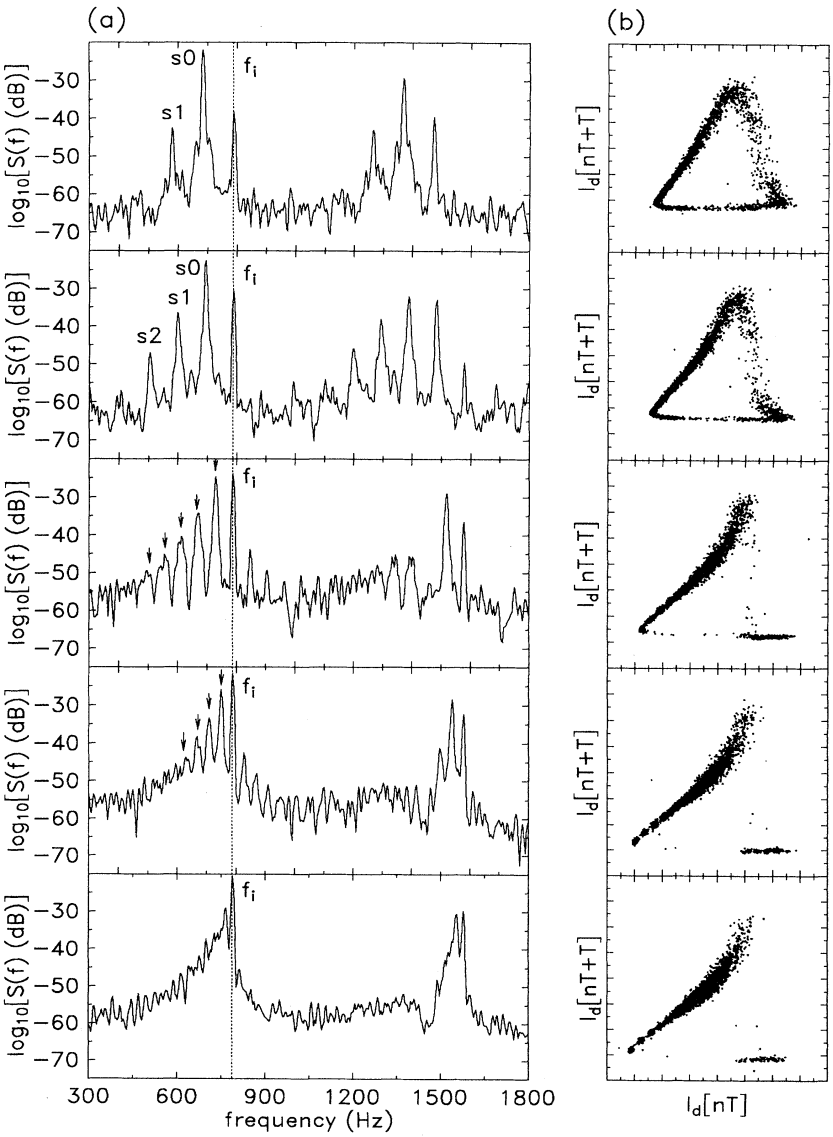

FIG. 12. Experimental study of power spectra of the system's response if the driving force is increased (from the top to the bottom figure) while the driving frequency is kept constant. The left column (a) shows the power spectra of the system response, the right column (b) the stroboscopic mapping of the corresponding phase space. The sidebands in the power spectra are either labeled or indicated by arrows. With the increase of the driving force, more and more sidebands appear and the beat frequency decreases. In the stroboscopic mapping, with increasing driving force, the closed cycle gets less homogeneously covered until most of the trajectories pass a neighborhood of the fixed point.

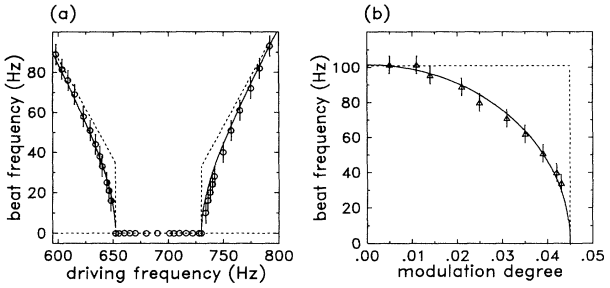

FIG. 13. (a) Beat frequency Ω for a horizontal cut (increase of the driving frequency) across the Arnol'd tongue with periodicity $P = 1$ and theoretical prediction (solid line) as calculated from Eq. (8). For comparison, the conventional beat frequency $\Omega_0 = \omega_i - \omega_0$ is shown (dashed line). (b) Observed shift of the beat frequency Ω as the Arnol'd tongue is approached by an increase of the driving voltage. For comparison, the theoretically predicted dependence, given by Eq. (8), is included in the graph (solid line). The conventional beat frequency is indicated by the dashed line.

of the driven discharge [31]. This fact is demonstrated in Fig. 16(a) where the time series of an entrained state with periodicity one are compiled with a common time axis (external driving voltage, discharge current, plasma potential, and total particle numbers). Both plasma potential and discharge current maintain a constant phase relative to the driving force, with the maxima in I_d and ϕ_p being simultanous with the minima of the driving force. The oscillation of the total particle numbers has a fairly small amplitude and is entrained to the driving force.

It is revealing to compare the set of time series of entrainment with that of periodic pulling [Fig. 16(b)]. During one beat cycle, the phase relationships between the driving force and both discharge current and plasma potential continuously shift until the characteristic phase condition for entrained states is fullfilled again (cf. fifth period). The key information provided by the simulation calculations is the temporal evolution of the total particle numbers during a beat cycle: In the first three driving-force periods, the phase relationship between the external driver and the self-oscillation causes a strong variation in the total particle numbers (about 15% for electrons and 20% for ions). At the fourth driving-force period, the relative phase between the external modulation and the internal oscillation results in a reduced particle loss in the discharge. Hence the subsequent refilling procedure leads to significantly higher particle numbers and the conditions for the instability of the potential structure are met much earlier [31,32]. Between the fourth and fifth driving-force periods, the development of each fluctuating quantity matches the behavior associated with the entrained case shown in Fig. 16(a). However, the entrained state is not preserved because the driving force is still too weak to control the total particle numbers beyond one driving-force period. Consequently, the sequence described above repeats periodically. Temporal evolution in this descriptive model parallels that of the

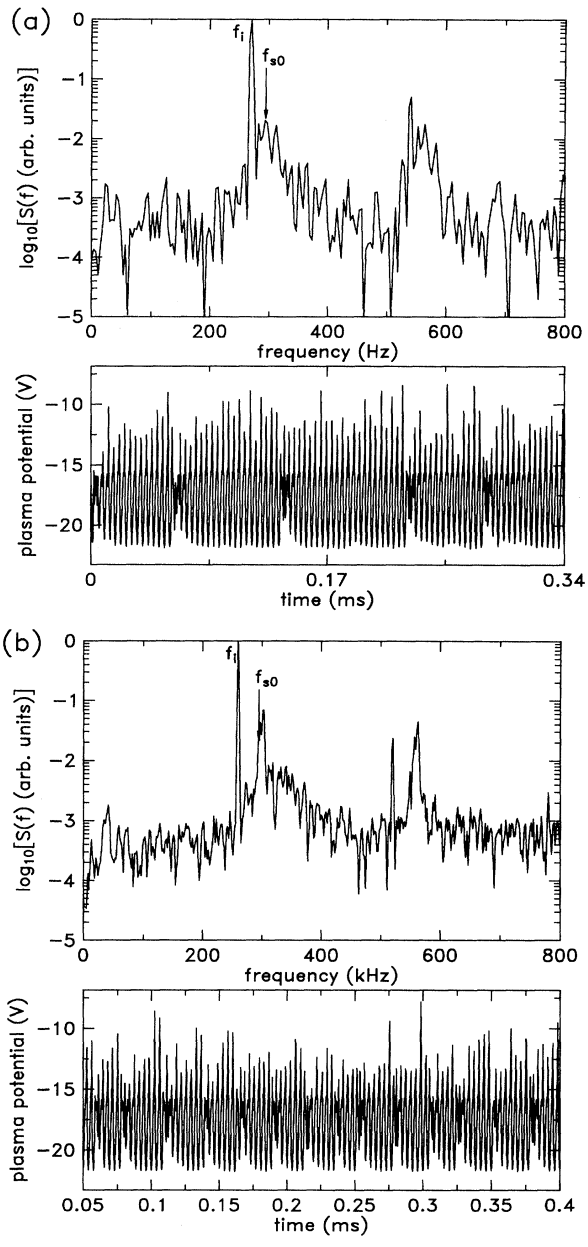

FIG. 14. Particle-in-cell simulation of the periodically driven thermionic discharge shows a clear indication of periodic pulling. (a) Strong periodic pulling close to the Arnol'd tongue. The power spectrum of the system's response (top) is single sided, the time series of the midplane plasma potential (bottom) shows periodic beats with a nonsinusoidal envelope. (b) Less pronounced periodic pulling. The power spectrum (top) is still asymmetric with respect to the zeroth-order sideband. The time series of the midplane potential (bottom) is characterized by the higher beat frequency.

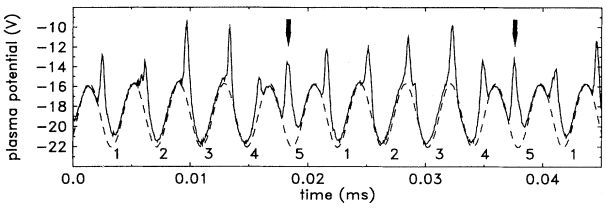

FIG. 15. A typical single beat cycle of pronounced periodic pulling as obtained from the particle-in-cell simulation of the thermionic discharge. The driving signal (dashed line) and the index number of full periods per beat cycle are included in the diagram. The arrows indicate the end of each beat cycle.

experimental observations and thus may be a viable explanation of periodic pulling in the driven thermionic discharge.

The undriven self-oscillation process involves a synchronization of several plasma and discharge parameters, i.e., plasma length, total ion number, and the electron drift velocity. During each current oscillation cycle, these parameters develop in a well-defined way until a particular instability criterion is met [31]. Because of the interrelationship of these time-dependent parameters, it is difficult to judge the relative importance of each of them with respect to the onset of the instability. With a periodic modulation of the discharge voltage, at a frequency close to the frequency of the self-oscillation, the instability of the plasma can also be triggered by the external force. Basically, this process is independent from the time evolution of the set of parameters mentioned above. Thus the analysis of periodic pulling via computer simulations presents one with a unique opportunity to recognize which criteria are always met preceding the instability and which conditions only appear critical from viewing the undriven and entrained systems. From the analysis presented above, it is apparent that the properties of the electron distribution function are more strongly correlated with the onset of the instability than other parameters. The inspection of the time evolution of parameters [Fig. 16(a), entrained state and Fig. 16(b), periodic-pulling state] clearly demonstrates that periodic pulling consists of a quasiperiodic regime followed by a transition to an entrained state, as predicted by the vdP model (cf. also Fig. 4).

VI. SUMMARY AND CONCLUSIONS

The periodic-pulling phenomenon is observed for a potential-relaxation oscillation in a thermionic discharge, both in an experiment and in a PIC simulation. The dynamics of (strong) periodic pulling are distinguished from the dynamics of quasiperiodicity (weak periodic pulling) and entrainment by inspection of the time series, power spectrum, phase evolution, and stroboscopic mapping, as interpreted using analytical vdP theory. The experimentally measured distortion in the beat frequency due to the nonlinear process is in good agreement with predictions from vdP theory. The results from computer simulations reinforce the interpretation of the experiment and provide insight into the microphysics of the nonlinear process. On the one hand, both experimental data and

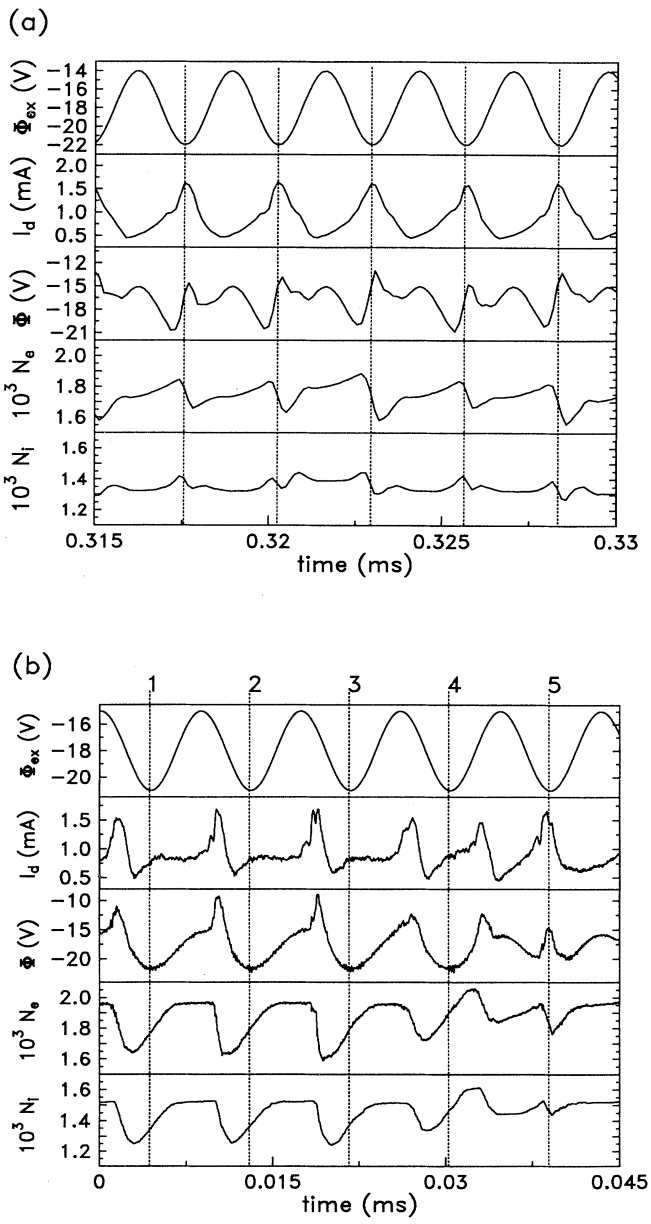

FIG. 16. Time series generated by the particle-in-cell simulation. From top to bottom: external driving signal $\Phi_{ex}(t)$, discharge current $I_d(t)$, midplane plasma potential $\Phi(t)$, total number of electron superparticles $N_e(t)$, and total number of ion superparticles $N_i(t)$. Shown are a frequency entrainment (a) and periodic pulling (b). The numbers in (b) correspond to the numbering of full periods in Fig. 15.

computer simulation exhibit the primary characteristic of nonsinusoidal frequency modulation (in the appearances of spikes in discharge current I_d and midplane plasma potential ϕ_m) and the asymmetric power spectrum. On the other hand, the computer simulation shows how the process of particle accumulation and loss and the creation of temporary structures in the electrostatic potential explain the physics of periodic pulling in the thermionic discharge.

ACKNOWLEDGMENTS

This work was performed under the auspices of DFG Sonderforschungsbereich 198/A8 "Kinetik partiell ionisierter Plasmen" and the U.S. National Science Foundation. One author (M.E.K.) would like to acknowledge travel support from these agencies and the kind hospitality of the Kiel plasma physics group during his stay.

[1] T. Kapitaniak, *Chaotic Oscillators* (World Scientific, Singapore, 1992).
[2] B. van der Pol, Philos. Mag. **43**, 700 (1922).
[3] B. van der Pol, Philos. Mag. **3**, 65 (1927).
[4] C. Hayashi, *Nonlinear Oscillations in Physical Systems* (Princeton University Press, Princeton, NJ, 1964).
[5] K. Kurokawa, Proc. IEEE **61**, 1386 (1973).
[6] R. H. Abraham and H. B. Stewart, Physica D **21**, 394 (1986).
[7] U. Parlitz and W. Lauterborn, Phys. Rev. A **36**, 1428 (1987).
[8] R. Mettin, U. Parlitz, and W. Lauterborn, Int. J. Bifurcation Chaos **3**, 1529 (1993).
[9] B. E. Keen and W. H. W. Fletcher, Phys. Rev. Lett. **23**, 760 (1969).
[10] B. E. Keen and W. H. W. Fletcher, J. Phys. D **3**, 1868 (1970).
[11] Y. Nakamura, J. Phys. Soc. Jpn. **25**, 1315 (1970).
[12] Y. Nakamura, J. Phys. Soc. Jpn. **31**, 273 (1971).
[13] T. Tsuru, J. Phys. Soc. Jpn. **40**, 548 (1976).
[14] K. Ohe and S. Takeda, Jpn. J. Appl. Phys. **11**, 1173 (1972).
[15] K. Ohe and S. Takeda, Beitr. Plasma Phys. **14**, 55 (1974).
[16] P. Michelsen, H. L. Pécseli, J. J. Rasmussen, and R. Schrittwieser, Plasma Phys. **21**, 61 (1979).
[17] T. Gyergyek, M. Čerček, N. Jelić, and M. Stanojević, Phys. Lett. A **177**, 54 (1993).
[18] H. Amemiya, Beitr. Plasma Phys. **21**, 195 (1981).
[19] H. Amemiya, Plasma Phys. **25**, 735 (1983).
[20] H. Lashinsky, in *Symposium on Turbulence of Fluids and Plasmas*, Polytechnic Institute of Brooklyn, edited by J. Fox (Polytechnic Press, New York, 1968), pp. 29–46.
[21] M. E. Koepke and D. M. Hartley, Phys. Rev. A **44**, 6877 (1991).
[22] M. E. Koepke, T. E. Sheridan, and M. J. Alport, in *Physics of Space Plasmas (1992)*, edited by T. Chang, G. B. Crew, and J. R. Jasperse (Scientific, Cambridge, MA, 1993), pp. 551–558.
[23] T. E. Sheridan, M. E. Koepke, C. A. Selcher, and T. N. Good, Proc. SPIE **2039**, 158 (1993).
[24] R. H. Abrams, E. J. Yadlowsky, and H. Lashinsky, Phys. Rev. Lett. **22**, 275 (1969).
[25] M. E. Koepke, M. J. Alport, T. E. Sheridan, W. E. Amatucci, and J. J. Carroll III, Geophys. Res. Lett. **21**, 1011 (1994).
[26] T. Klinger, A. Piel, F. Seddighi, and C. Wilke, Phys. Lett. A **182**, 312 (1993).
[27] H. Lashinsky, T. J. Rosenberg, and D. L. Detrick, Geophys. Res. Lett. **7**, 837 (1980).
[28] S. Iizuka *et al.*, Phys. Rev. Lett. **48**, 145 (1982).
[29] F. Bauer and H. Schamel, Physica D **54**, 235 (1992).
[30] F. Greiner, T. Klinger, H. Klostermann, and A. Piel, Phys. Rev. Lett. **70**, 3071 (1993).
[31] F. Greiner, T. Klinger, and A. Piel, Phys. Plasmas **2**, 1810 (1995).
[32] T. Klinger, F. Greiner, A. Rohde, and A. Piel, Phys. Plasmas **2**, 1822 (1995).
[33] N. N. Bogoljubow and J. A. Mitropolski, *Asymptotic Methods in the Theory of Nonlinear Oscillations* (Gordon and Breach, New York, 1961).
[34] R. Adler, Proc. IRE **34**, 351 (1946).
[35] M. Armand, Proc. IEEE **57**, 798 (1969).
[36] M. E. Koepke, in *Physics of Space Plasmas (1991)*, edited by T. Chang, G. B. Crew, and J. R. Jasperse (Scientific, Cambridge, MA, 1992), p. 393.
[37] E. A. Jackson, *Perspectives of Nonlinear Dynamics* (Cambridge University Press, Cambridge, England, 1991), Vol. 1.
[38] R. Seydel, *From Equilibrium to Chaos* (Elsevier Science Publishing, Amsterdam, 1988).
[39] N. Hershkowitz, in *Plasma Diagnostics*, edited by O. Auciello and D. L. Flamm (Academic Press, New York, 1993), Vol. 1.
[40] R. L. Merlino and S. L. Cartier, Appl. Phys. Lett. **44**, 33 (1984).
[41] J. R. Pierce, J. Appl. Phys. **15**, 721 (1944).
[42] P. Y. Cheung and A. Y. Wong, Phys. Rev. Lett. **59**, 551 (1987).
[43] S. Kuhn, Contrib. Plasma Phys. **34**, 495 (1994).
[44] C. K. Birdsall, IEEE Trans. Plasma Sci. **19**, 65 (1991).
[45] J. Verboncœr, V. Vahedi, M. V. Aleves, and C. K. Birdsall, *PDP1 Plasma Device Planar 1-Dimensional Bounded Electrostatic Code* (Plasma Physics and Simulation Group, University of California, Berkeley, 1990).
[46] F. Greiner, T. Klinger, A. Piel, and R. Timm, in *Proceedings of the Fourth Symposium on Double Layers and Other Nonlinear Phenomena in Plasmas*, edited by R. W. Schrittwieser (World Scientific, Singapore, 1993), pp. 208–213.

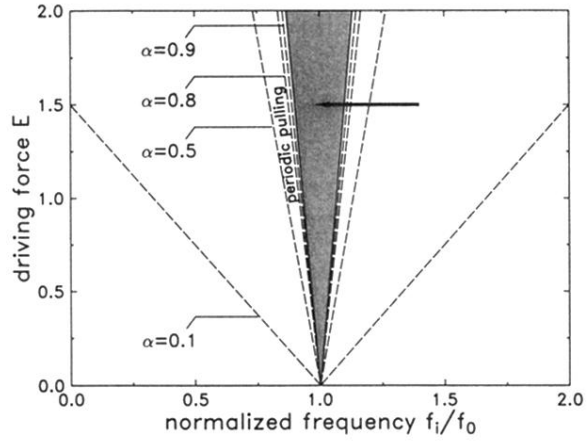

FIG. 2. Arnol'd tongue for the frequency-entrained states of periodicity one (shaded region). The dashed lines correspond to different entrainment parameters α and indicate lines of equally marked periodic pulling. The numerical and experimental investigations of the periodic-pulling phenomenon are performed by decreasing the driving frequency while the driving force is kept constant, as indicated by the arrow.